Latitudinal gradient in the respiration quotient and the implications for ocean oxygen availability

Allison R. Moreno[a], Catherine A. Garcia[b], Alyse A. Larkin[b], Jenna A. Lee[b], Wei-Lei Wang[b], J. Keith Moore[b], Francois W. Primeau[b], and Adam C. Martiny[a,b,1]

[a]Department of Ecology and Evolutionary Biology, University of California, Irvine, CA 92697; and [b]Department of Earth System Science, University of California, Irvine, CA 92697

Edited by Donald E. Canfield, Institute of Biology and Nordic Center for Earth Evolution, University of Southern Denmark, Odense M., Denmark, and approved July 28, 2020 (received for review March 23, 2020)

Climate-driven depletion of ocean oxygen strongly impacts the global cycles of carbon and nutrients as well as the survival of many animal species. One of the main uncertainties in predicting changes to marine oxygen levels is the regulation of the biological respiration demand associated with the biological pump. Derived from the Redfield ratio, the molar ratio of oxygen to organic carbon consumed during respiration (i.e., the respiration quotient, $r_{-O2:C}$) is consistently assumed constant but rarely, if ever, measured. Using a prognostic Earth system model, we show that a 0.1 increase in the respiration quotient from 1.0 leads to a 2.3% decline in global oxygen, a large expansion of low-oxygen zones, additional water column denitrification of 38 Tg N/y, and the loss of fixed nitrogen and carbon production in the ocean. We then present direct chemical measurements of $r_{-O2:C}$ using a Pacific Ocean meridional transect crossing all major surface biome types. The observed $r_{-O2:C}$ has a positive correlation with temperature, and regional mean values differ significantly from Redfield proportions. Finally, an independent global inverse model analysis constrained with nutrients, oxygen, and carbon concentrations supports a positive temperature dependence of $r_{-O2:C}$ in exported organic matter. We provide evidence against the common assumption of a static biological link between the respiration of organic carbon and the consumption of oxygen. Furthermore, the model simulations suggest that a changing respiration quotient will impact multiple biogeochemical cycles and that future warming can lead to more intense deoxygenation than previously anticipated.

Redfield ratio | CESM | inverse modeling | elemental stoichiometry | photosynthetic quotient

The oceans are currently experiencing deoxygenation and an expansion of oxygen minimum zones (1) with potentially devastating impacts on marine life (2). Warming induced changes in oxygen solubility as well as circulation-driven ventilation rates are considered the primary drivers of deoxygenation (3). However, current models are unable to reproduce observed shifts in ocean oxygen concentrations (4).

One of the main uncertainties in predicting ocean oxygen levels is the regulation of the biological respiration demand (5). The respiration quotient describes the molar ratio of oxygen to organic carbon consumed during respiration and is thus controlled by the oxidation state of organic material (signified by z) (6),

$$C_x(H_2O)_w(NH_3)_yH_zH_3PO_4 + \left(x + \frac{1}{4}z\right)O_2 \rightarrow xCO_2 + y \quad NH_3 + H_3PO_4 + \left(w + \frac{1}{2}z\right)H_2O, \quad [1]$$

$$r_{-O2:C} = \frac{(x + \frac{1}{4}z)}{x}, \quad [2]$$

with an additional oxygen demand due to nitrification,

$$y\ NH_3 + 2y\ O_2 \rightarrow y\ HNO_3 + y\ H_2O, \quad [3]$$

yielding the total respiration quotient ($r_{\Sigma-O2:C}$) describing the full oxidation of particulate organic matter,

$$r_{\Sigma-O2:C} = \frac{(x + \frac{1}{4}z + 2y)}{x}. \quad [4]$$

The respiration quotient is commonly prescribed within models to be static. Alfred Redfield implicitly assumed that all planktonic organic carbon consisted of carbohydrates (setting z to zero), and thus, $r_{-O2:C} = 1.0$ and $r_{\Sigma-O2:C} = 1.3$ (7). Carbohydrates represent a somewhat oxidized form of organic carbon, and other macromolecules (especially lipids) are further reduced with higher $r_{-O2:C}$. Nevertheless, theoretical estimations of phytoplankton biomass chemistry independently predicted the respiration quotient to be ~1.1 with limited biological variation (8, 9). Finally, a recent analysis using satellite-derived macromolecular composition of phytoplankton and gridded nutrient data were unable to detect any systematic geospatial variation (10). Based on these considerations, ocean biogeochemical models and theories assume a constant respiration quotient, although they disagree on the exact value (6).

There is also evidence suggesting substantial variation in the respiration quotient. First, the macromolecular composition of

Significance

The loss of ocean oxygen caused by climate warming is a serious environmental issue and could lead to major declines in animal habitats. However, current Earth system models struggle in explaining observed trends in global ocean oxygen. Using a model, we demonstrate that marine oxygen concentrations depend sensitively on a rarely considered quantity known as the respiration quotient to prescribe the oxygen consumed per mole of organic carbon respired. Using a combination of direct chemical measurements across major biomes in the eastern Pacific Ocean plus changes in the global distribution of oxygen and carbon, we show how the respiration quotient increases systematically with temperature. The findings imply that we can experience more intense declines in ocean oxygen with warming.

Author contributions: A.R.M., F.W.P., and A.C.M. designed research; A.R.M., C.A.G., A.A.L., J.A.L., W.-L.W., J.K.M., F.W.P., and A.C.M. performed research; J.K.M. contributed new reagents/analytic tools; A.R.M., F.W.P., and A.C.M. analyzed data; and A.R.M. and A.C.M. wrote the paper.

The authors declare no competing interest.

This article is a PNAS Direct Submission.

[1]To whom correspondence may be addressed. Email: amartiny@uci.edu.

This article contains supporting information online at https://www.pnas.org/lookup/suppl/doi:10.1073/pnas.2004986117/-/DCSupplemental.

First published August 31, 2020.

plankton differs across lineages (11) and physiological states (12) leading to a large predicted biological variation in the respiration quotient (*SI Appendix*, Fig. S1). Second, a limited set of full elemental analyses of particulate organic matter provides support for variation in the carbon oxidation state (13, 14). Third, end-member mixing models of oxygen and DIC concentrations along isopycnal surfaces suggest large variance in $r_{-O2:C}$ between ocean basins (15). However, this method can have large biases (16). Fourth, global inverse model studies find large-scale gradients in $r_{-O2:P}$ and $r_{C:P}$ for the regeneration of organic matter (17, 18). Simply dividing these two ratios suggests that $r_{\Sigma-O2:C}$ could range between 0.7 and 2.1. Such independent studies challenge the notion of a static link between the oxygen and carbon cycles, but the drivers, magnitude, and regional differences of the respiration quotient are unknown.

Here we report the outcome from a set of prognostic ocean biogeochemical model simulations, direct chemical measurements of the respiration quotient from diverse biomes, and a global inverse model analysis to address the following research questions: 1) what are the global biogeochemical implications of a changing $r_{-O2:C}$, 2) what is the regional average and variation in $r_{-O2:C}$, and 3) does the regional variation in $r_{-O2:C}$ systematically relate to specific environmental conditions?

Results

A change in the respiration quotient can have widespread impacts on ocean oxygen, nitrogen, and carbon cycle processes. We conducted sensitivity simulations with a prognostic global ocean biogeochemical model (19). The Community Earth System Model (CESM) allowed for variation and dynamical feedbacks between the carbon, nitrogen, oxygen, and phosphorus cycles and included the regulation of primary production, carbon export, and an oxygen-dependent water column and sediment denitrification. We varied $r_{-O2:C}$ between 0.7 and 1.3 to test for potential biogeochemical impacts of a changing respiration quotient. After a 300 y spin-up period using unique respiration quotients, we observed nearly linear relationships between $r_{-O2:C}$ and ocean oxygen content, water column denitrification, and carbon productivity (Fig. 1). The model sensitivity analysis showed that increasing the respiration quotient by 0.1 from our control ($r_{-O2:C} = 1$) will result in an average loss of 0.15×10^{18} g oxygen (2.3%) and a 58% expansion of oxygen minimum zones (OMZ) (<25 μmol/kg O_2) (Fig. 1 *A*–*C*). The annual rate of water column denitrification and overall N balance in the ocean were sensitive to the respiration quotient (Fig. 1 *D*–*F*). Thus, increasing the respiration quotient by 0.1 leads to elevated water column denitrification of 38 Tg N and thus changed this rate substantially. Water column denitrification ranged from 3 to 277 Tg N/y across our simulations but nearly shut down at $r_{-O2:C} = 0.7$ or rose to very high levels at $r_{-O2:C} = 1.3$. Indirectly, through the loss of fixed N, an increase in $r_{-O2:C}$ of 0.1 lowered net primary productivity and export production slightly by an average 0.86 (1.59%) and 0.13 (1.56%) Pg C/y, respectively (Fig. 1 *G* and *H*). These carbon cycle feedbacks were particularly pronounced on the edge of existing OMZs. Thus, the respiration quotient is an important regulator of marine biogeochemical cycles.

The changes to ocean biogeochemical cycles from a varying respiration quotient are comparable in magnitude to business-as-usual climate change impacts by year 2100 (*SI Appendix*, Fig. S2 and Table S1). Climate simulations performed under scenario Representative Concentration Pathway 8.5 (RCP8.5) showed a decline in the total dissolved oxygen content of the ocean between 3.1 and 4.7% by year 2100. A change in $r_{-O2:C}$ of ∼0.2 in CESM simulations resulted in equivalent oxygen changes (Fig. 1). Therefore, a shift in the respiration quotients can significantly impact ocean oxygen levels and biogeochemical cycles more broadly.

To directly quantify the respiration quotient, we combined field measurements of particulate organic carbon (POC) and the required oxygen demand for respiration across a meridional transect in the eastern Pacific Ocean. POC was estimated by combustion and the release of CO_2 using an elemental analyzer. To quantify the oxygen required for complete respiration of POC, we modified and calibrated a method commonly used for measuring the particulate chemical oxygen demand (PCOD) in wastewater (20). We then estimated the respiration quotient ($r_{-O2:C}$) by taking the ratio of PCOD and POC across 198 stations along the Pacific Ocean line P18 (*SI Appendix*, Table S2). Sea surface temperature steadily decreased from 29.5 to ∼0 °C (Fig. 2*A*). A deep nutricline was detected in multiple regions marking the location of oligotrophic conditions (Fig. 2*B*). Nitrate was mostly drawn down to detection limit in several regions, whereas residual phosphate was present throughout the eastern Pacific Ocean (*SI Appendix*, Fig. S4). As a result, N* was low in most of the tropical and subtropical regions but rose with the high nutrient supply in the Southern Ocean (Fig. 2*C*). As such, our samples covered a broad range of environmental conditions across the eastern Pacific Ocean.

We observed distinct but highly correlated particulate organic matter (POM) concentration levels across the regions. [POC] and [PCOD] were tightly correlated ($r^2_{Pearson} = 0.93$, $P < 0.0001$) (Fig. 2 *D* and *E*) and showed parallel regional shifts. Thus, our optimized PCOD assay accurately reflects the amount of oxygen required to oxidize all nonnitrogenous compounds making up marine particulate organic matter. [POC] and [PCOD] were low in regions with a deeper nutricline (1, Central American Coast [CAMR]; 2, North Pacific Equatorial Counter Current [PNEC]; 3, Transitional Pacific Equatorial Divergence [TPEQ]; and 5, South Pacific Gyre [SPSG]), slightly higher in equatorial Pacific Ocean waters (4, Pacific Equatorial Divergence [PEQD]), and very high in the Southern Ocean regions (6, Southern Subtropical Convergence [SST] to 9, Austral Polar [APLR]) (Fig. 2 *D* and *E*). Changes in POM concentrations followed the nine regions that arose from the combination of environmental conditions. $r_{-O2:C}$ averaged $1.15^{1.54}_{0.73}$ (minimum and maximum value) (Fig. 2*F* and *SI Appendix*, Table S3) but differed significantly between regions ($p_{MANOVA} < 6 \times 10^{-5}$) (Fig. 3). The highest and lowest regional averages were found near the warm edge of the North Pacific Subtropical Gyre and the ice edge in the Southern Ocean, respectively. The equatorial regions were also slightly lower compared to the coastal/counter current and gyre regions. Many regions showed limited overlap with the respiration quotient defined by Redfield or Anderson but instead largely separated along a latitudinal gradient (Fig. 3). Thus, the observed respiration quotient showed regional shifts leading to a common divergence from past predicted values.

We observed a significant correspondence between ocean environmental conditions and the respiration quotient. We tested all linear combinations of environmental factors and $r_{-O2:C}$ (*SI Appendix*, Table S4). A significant positive relationship between temperature and $r_{-O2:C}$ suggested an increase in $r_{-O2:C}$ of ∼0.2 between polar and tropical regions (Fig. 4*A*). We saw indications of an additional regulation of $r_{-O2:C}$ by nutrient availability (*SI Appendix*, Table S4). A deeper nutricline led to a slightly elevated quotient in comparison to waters with the same temperature but higher nutrients (e.g., the equatorial region). A positive relationship between temperature and the respiration quotient was also observed for a small set of previously analyzed samples from the western North Pacific Ocean (*SI Appendix*, Fig. S5). Overall, temperature emerged as the best predictor, but additional factors may exert a secondary control on the respiration quotient.

We tested if the observed temperature dependence of $r_{-O2:C}$ could be detected via the imprint on the global three-dimensional (3D) distribution of oxygen and dissolved inorganic carbon in the

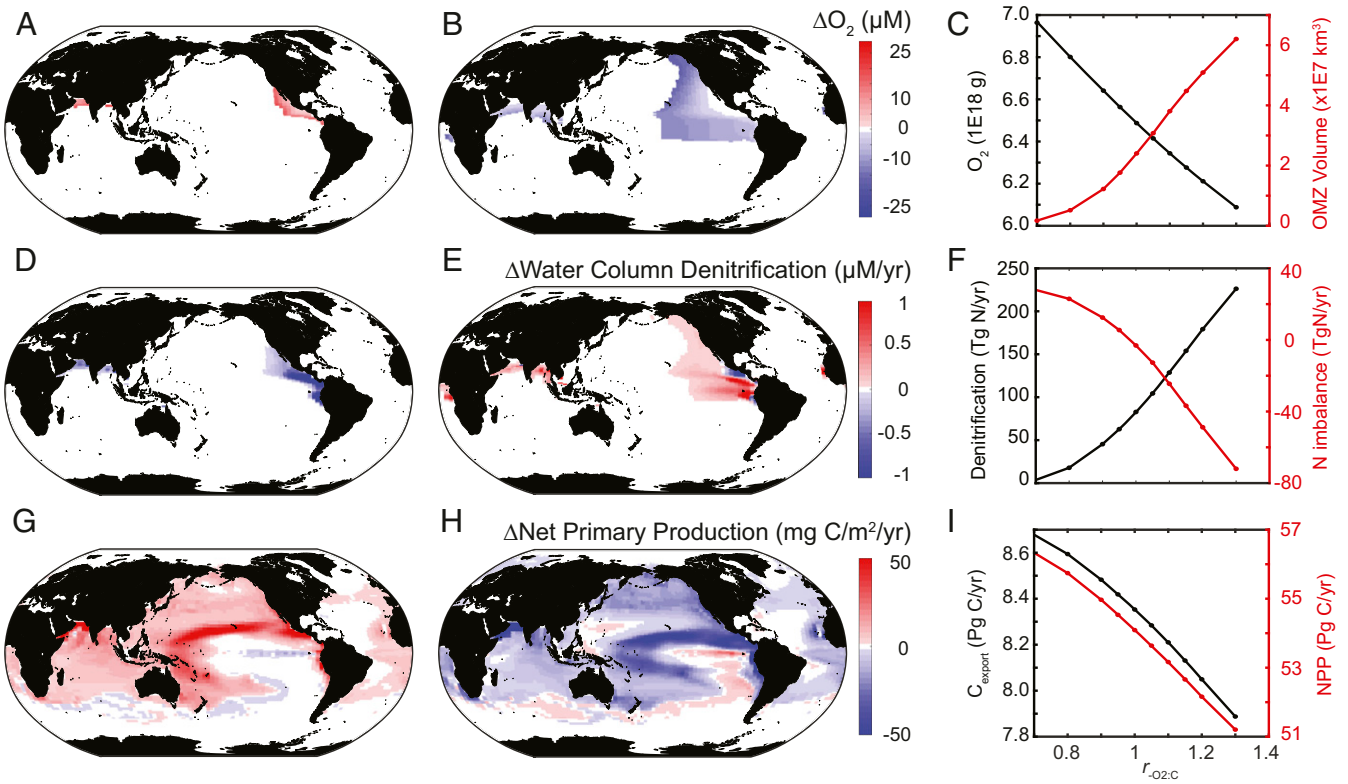

Fig. 1. Impact of a changing respiration quotient on ocean biogeochemical processes. (*A*) Change in OMZ ($O_2 \leq 25$ μM) extent and intensification when $r_{-O2:C}$ shifts from 1 to 0.7. (*B*) Change in OMZ extent and intensification when $r_{-O2:C}$ shifts from 1 to 1.3. (*C*) Total oxygen levels and OMZ volume ($[O_2] < 25$ μM) as a function of the respiration quotient. (*D*) Change in water column denitrification zones and intensity when $r_{-O2:C}$ shifts from 1 to 0.7. (*E*) Change in water column denitrification zones and intensity when $r_{-O2:C}$ shifts from 1 to 1.3. (*F*) Annual water column denitrification rates and global ocean N balance as a function of the respiration quotient. (*G*) Change in ocean net primary production when $r_{-O2:C}$ shifts from 1 to 0.7. (*H*) Change in ocean net primary production when $r_{-O2:C}$ shifts from 1 to 1.3. (*I*) Annual net primary production and carbon export (at 100 m) as a function of the respiration quotient.

ocean. To achieve this, we constructed an inverse biogeochemical model constrained by the GLODAP.2016v2 and WOA2013 databases of hydrographic measurements of nutrients, carbon, and oxygen concentrations (21, 22). We relied on previous inverse-modeling efforts for the carbon, nitrogen, and phosphorus cycles (18, 19, 23) but with an added oxygen cycling model. The resulting biogeochemical model tracks the dissolved oxygen concentration as well as the oxidation and reduction of both nitrogen and carbon. Based on the direct chemical measurements, we introduced a linear sea-surface temperature dependence of the respiration quotient but with unknown slope and intercept. We then estimated $r_{-O2:C} = 0.974^{0.980}_{0.968}$ at 15 °C (± 1 SD) and a positive temperature dependence of $0.0162^{0.0167}_{0.0157}$ °C^{-1} through a Bayesian inversion procedure against the global 3D distribution of nutrients, carbon, and oxygen concentrations (Fig. 4*B*). The sea-surface temperature dependence of $r_{-O2:C}$ from the inverse model is stronger, with better fits in warmer waters and weaker fits in cooler waters. However, the chemical measurements and inverse hydrographic estimate both agree on a positive temperature relationship and the level at higher temperatures (Fig. 4). We also evaluated a nitrate-based model for $r_{-O2:C}$, but there was stronger support for a temperature dependence (*SI Appendix*). We allowed for independent remineralization depth profiles (Martin's *b*) of POC and PCOD. b_{Oxygen} was slightly smaller than b_{Carbon} suggesting that oxygen was consumed deeper in the water column compared to the release of DIC. However, the uncertainty in each parameter led to overlapping values, so it was unclear if the carbon and oxygen remineralization profiles were truly distinct. The midpoint value of $r_{-O2:C}$ at 15 °C was also sensitive to the inclusion of separate Martin's *b* values for POC and PCOD. A separate inverse model with a common depth profile for POC and PCOD yielded a mean $r_{-O2:C}$ value of 1.12, which is in better agreement with the value measured directly in suspended particles. This link suggested some poorly constrained model interactions between the mean respiration quotient and the remineralization depth profiles. However, the positive temperature dependence of $r_{-O2:C}$ was retained independently of how we parameterized remineralization depth profiles. In summary, we have convergent estimates of a regional temperature-related respiration quotient but uncertainty in the magnitude of change.

Discussion

The observed range for the respiration quotient is slightly outside the bounds of predictions based on cellular biochemistry (8, 9). However, the C:H:O ratio of POM in the western Pacific Ocean corresponds to a calculated respiration quotient ranging between 0.6 and 1.6 (13), and several studies have measured 40% variation in C:H (24). Platt and Irwin observed a 30% variation in the caloric content of fresh organic matter (25). As the carbon oxidation state and caloric content of organic matter are closely tied (24), one should expect a parallel range in the respiration quotient. Part of POM is detrital matter with molecularly uncharacterized components (26) that could lead to higher $r_{-O2:C}$ variation than predicted purely from cellular biochemistry arguments. The observed values are also within the bounds from end-member mixing models (15) and other POM

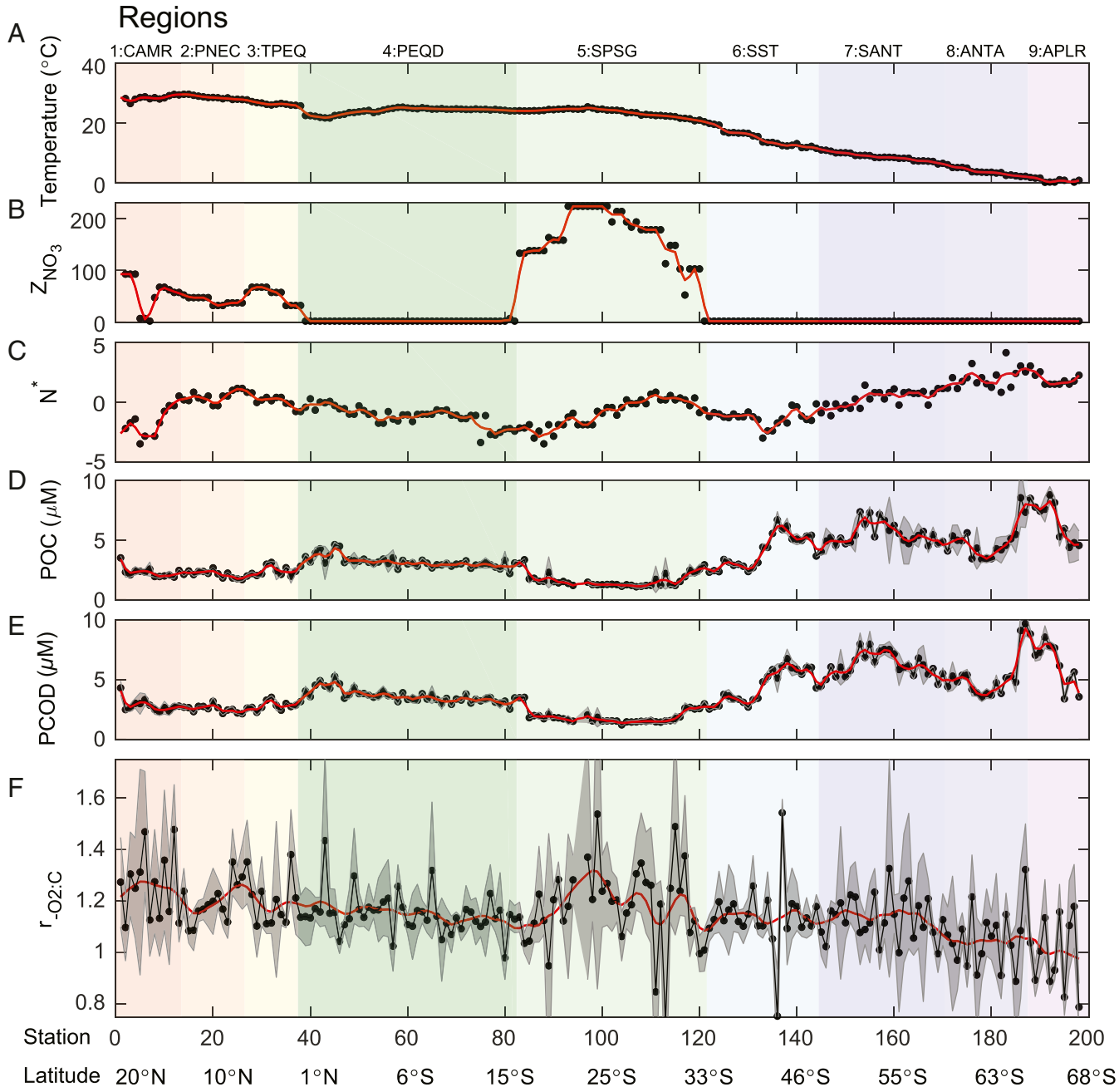

Fig. 2. Environmental conditions, POM concentrations, and the respiration quotient across the eastern Pacific Ocean. (*A*) Sea surface temperature. (*B*) Nutricline depth (depth at which nitrate is 1 μM). (*C*) Surface N* (N* = $NO^{-3}_{Station} - 16*PO4^{-3}_{Station}$). (*D*) Surface POC. (*E*) Surface PCOD. (*F*) Surface respiration quotient. Averaged data are marked as black dots. In *A*–*E*, the red line represents a four-station moving average. In *D*–*F*, the gray shaded regions represent the SD of the replicates. In *F*, the red line represents an eight-station moving average. In all panels, the colored background represents the nine regions (1, CAMR; 2, PNEC; 3, TPEQ; 4, PEQD; 5, SPSG; 6, SST; 7, Sub-Antarctic water ring [SANT]; 8, ANTA [Antarctic]; and 9, APLR).

analyses (13). Thus, our detected range in $r_{-O2:C}$ is high but falls within past observations of particulate organic matter.

The observed latitudinal gradient for the respiration quotient must be linked to changes in the underlying molecular composition of surface POM and plankton. The exact nature of this relationship is not known but possibly driven by an increased proportion of lipids relative to proteins and carbohydrates. The plankton communities are distinct between the analyzed regions in the eastern Pacific Ocean suggesting that environmentally driven community shifts at least partially contribute to the variation in the respiration quotient. The proportion of biochemical components across major phytoplankton groups follows an allometric relationship leading to an increased lipid-to-carbohydrate/protein ratio in small plankton (27). We speculate that smaller cells have a higher contribution of the lipid-rich membrane to total carbon due to the elevated surface-to-volume ratio. Thus, the high abundance of small picoplankton in warm tropical and subtropical regions can therefore lead to a higher lipid fraction and higher respiration quotient of the organic matter. Another biological mechanism is the accumulation of lipids following a nitrogen starvation response in many phytoplankton (28), and we observed the highest respiration quotient in warm regions with a deep

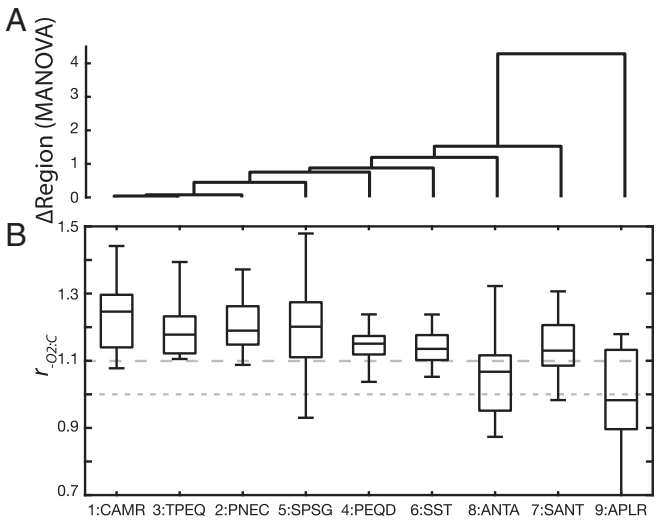

Fig. 3. Regional differences in the respiration quotient. (*A*) Clustering of group means after a multivariate joint POC and PCOD analysis of variance (one-way MANOVA). (*B*) Regionally observed respiration quotients and comparisons to Redfield ($r_{-O2:C} = 1$) and Anderson ($r_{-O2:C} = 1.1$) theoretically predicted values.

nutricline. Thus, we hypothesize that shifts in plankton biogeography and possibly physiology influence the observed changes in the respiration quotient.

There are several noteworthy caveats to our conclusions. First, the POM oxidative state may change during sinking and aging leading to distinct remineralization length scales for DIC release and oxygen consumption. From the inverse model, we saw weak evidence for a faster attenuation of DIC compared to oxygen consumption suggesting a removal of oxidized compounds in the upper ocean. The confidence intervals for b_{Carbon} and b_{Oxygen} were overlapping, but future vertical joint profiles of POC and PCOD could further constrain any depth dependence of the respiration quotient. Second, we did not measure the respiration quotient of DOM even though this fraction is an important component of the ocean carbon cycle (29). Currently, no analytic methods can perform this measurement directly, so it is unclear if $r_{-O2:C}$ for POM and DOM will display the same level and biome patterns. Third, the simulated impact of a changing respiration quotient was limited to 300 y. Within the time scale most relevant to human society, the model analysis clearly emphasized the linear impact of the respiration quotient on ocean oxygen levels and downstream biogeochemical cascade. However, additional feedbacks could occur at longer time scales. Fourth, our observed variation in the respiration quotient in suspended POM and inferred from the inverse model shows variability that was not detected in another recent study (10). In this recent study, the respiration quotient was estimated by combining satellite-predicted macromolecular composition of surface POM and using a simple 1D model of hydrographic nutrient and oxygen measurements. This recent work may have lacked the sensitivity to detect regional shifts in $r_{-O2:C}$ as the lateral transport of nutrients and oxygen tends to dominate over 1D vertical transport in the ocean. Thus, our combination of a data-constrained 3D biogeochemical model (30) and direct POM measurements may be more sensitive for detecting a temperature dependence of $r_{-O2:C}$. Fifth, there is uncertainty embedded in our transport operator as well as in the global annual climatological description of hydrography that can impact the inverse model estimates. Seasonally resolved transport and biogeochemistry as well as expanded oxygen measurements from Biogeochemical-Argo floats will help further constrain future estimates of $r_{-O2:C}$. Sixth, $r_{-O2:C}$ may be related to additional parameters beyond temperature. For example, we saw indications of some impact of nutrient availability (although not as strong as temperature) as well as signs of daily variance possibly reflecting diel cycles in photosynthesis and cellular carbon accumulation. These sources of additional variance need to be addressed with expanded regional, vertical, and temporal sampling in future studies. The uncertainty estimates we have provided from our inverse model analysis are conditioned on the model structure. Exploring more complex relationships between $r_{-O2:C}$ and a broader suite of drivers in the laboratory, in situ, and by the inverse model should improve our understanding of how the respiration quotient is regulated. Nevertheless, our use of independent methods supports that the respiration quotient is not to be assumed constant but varies between biomes.

The observed variation in the respiration quotient is expected to have large biological and biogeochemical impacts. The production of more reduced organic carbon in tropical and subtropical regions implies a higher caloric content and perhaps a superior food source (24). On the other hand, we see that an upshift in the respiration quotient can initiate a biogeochemical cascade leading to lower ocean oxygen levels, N loss, and declining productivity. These biogeochemical changes could have

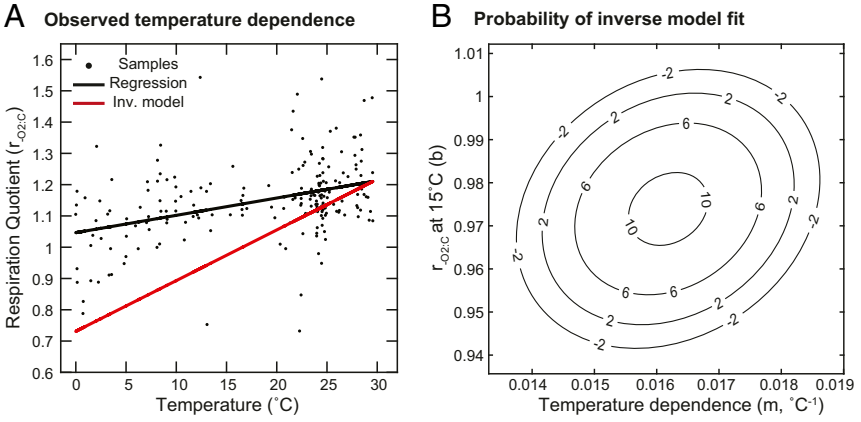

Fig. 4. Relationship between temperature and the respiration quotient. (*A*) Observed temperature dependence for surface POM $r_{-O2:C} = 1.0465 + (0.0055383/°C)$ *Temperature* (*SI Appendix*, Table S4) and the relationship inferred from the inversion of hydrographic data (*SI Appendix*, Table S6). (*B*) The logarithmic marginal posterior probability density for the temperature dependence (*m*) and intercept (*b*) in the relationship $r_{-O2:C} = m(Temperature - 15°C) + b$ estimated from the inversion of the hydrographic data.

devastating impacts on marine life (2). Thus, a biological feedback whereby warming and stratification lead to the production of more reduced organic carbon can have a large future impact on marine ecosystem functioning and biogeochemistry.

Materials and Methods

Sample Collection. Seawater samples were collected during the Global Ship-based Hydrographic Investigations Program (GO-SHIP) P18 cruise aboard R/V *Ronald H. Brown* from November 11, 2016, to February 3, 2017, between 32.72°N, 117.16°W off San Diego, CA, to 77.85°S, 166.67°E near Antarctica (*SI Appendix*, Fig. S3). Samples for POC and PCOD were taken from 198 stations using the underway system. The underway intake was located at a depth of 5.3 m from the sea surface. All carboys were rinsed twice with filtered seawater before sampling. Triplicate samples for POC and sextuplicate samples for PCOD were taken approximately three times daily. Water was prefiltered with a 30-μm nylon mesh (Small Parts no. 7050-1220-000-12) to remove rare large particles from the sample. Additional samples (triplicate for POC and sextuplicate for PCOD) were taken by removing the 30-μm nylon mesh, allowing all particles to collect in order to determine the total particulate organic matter from station 159 to 198. All samples were collected on precombusted 500 °C GF/F filters (Whatman, GE Healthcare) for the analysis of POC and PCOD. Sample volume was determined on a per station basis, ranging from 3 to 8 L. All filters were then folded in half, sealed inside precombusted aluminum foil, and stored at −20 °C until analysis.

POC. Filters were dried at 55 °C (24 h) and then stored in a desiccator with concentrated hydrochloric acid fumes for 24 h to remove inorganic carbonates. The filters were dried for 48 h at 55 °C before being folded and pelletized into precombusted tin capsules (CE Elantech). Tin capsules were then analyzed on a Flash EA 1112 NC Soil Analyzer (Thermo Scientific) measuring released CO_2, and we used an atropine ($C_{17}H_{23}NO_3$) standard.

PCOD Assay. Quantifying the chemical oxygen demand is commonly used for wastewater and freshwater samples. The assay is based on the determination of residual potassium dichromate following organic matter oxidation with silver sulfate as the catalyst under strongly acidic and high temperature (150 °C) conditions (20, 31, 32). As dichromate does not oxidize ammonium, the assay only quantifies the oxygen demand from organic carbon. A major obstacle for using the method with seawater POM samples is the interference of chloride ions. As such, chloride is oxidized by dichromate and causes precipitation of silver chloride. Several efforts have been made to apply this method to seawater samples, and the main solution is the addition of mercuric sulfate (33). Thus, the method has the potential for quantifying the oxygen demand in marine POM.

Here we modified the assay to quantify the chemical oxygen demand from POM collected on GF/F filters. Specifically, GF/F filters with collected POM samples were dried overnight at 55 °C. We then added the filter and 2 mL milli-Q water to HACH COD HR+ reagent vials (Product no. 2415915 containing mercuric sulfate) and digested the samples at 150 °C for 2 h. We learned that the major obstacle for this assay was uneven precipitation of silver chloride following digestion. Thus, we modified the assay to include a subsequent precipitation step by adding 92.1 μL of 9.5 M NaCl (minimum amount of chloride to induce consistent precipitation) to each vial. Vials were immediately inverted twice and centrifuged for 30 min at 2,500 rpm to remove any precipitate. Finally, we quantified the remaining dichromate by absorbance at 600 nm using HACH certified phthalate-based COD standards (*SI Appendix*, Fig. S6*A*). HACH certified COD tubes have been shown to measure unbiased COD across diverse classes of organic compounds (34) so we only did a limited comparison with other compounds.

To validate the modified technique, we 1) tested for any interference using standard additions of a HACH certified phthalate-based COD standard, 2) established a linear relationship between input amounts and absorbance, 3) compared the variance to other POM measurement techniques, and 4) examined any compound-specific biases. First, we were able to recover experimentally added organic carbon to seawater samples suggesting limited sample interference (*SI Appendix*, Fig. S6*B*). Second, we found that increasing sample volume (and associated amount of PCOD captured on filters) corresponded linearly to an increase in measured PCOD (*SI Appendix*, Fig. S6*C*). Third, we saw a high correspondence between theoretical and observed values for different substrates (*SI Appendix*, Fig. S6*D*). This has also been observed in more elaborate past studies supporting that the dichromate technique effectively oxidizes many diverse substrates (34, 35). Fourth, the coefficient of variance for PCOD and $r_{-O2:C}$ corresponded to the coefficient of variance for POC and $r_{C:P}$, respectively (*SI Appendix*, Fig. S6 *E*–*H*).

We did not fully explore the detection limit for our assay as the COD chemistry method was much more sensitive than one used for POC. Thus, our sampling strategy focused on recovering enough POC. These method development and optimization steps suggested that our assay provided an unbiased and sensitive method to quantify PCOD.

$r_{-O2:C}$ was computed from the mean concentrations of PCOD and POC. The SD for $r_{-O2:C}$ was calculated as a pooled sample:

$$\sigma_{r_{-O2:C}} = \frac{PCOD_{aver}}{POC_{aver}} \times \sqrt{\left(\left(\frac{\sigma_{PCOD}}{PCOD_{aver}}\right)^2 + \left(\frac{\sigma_{POC}}{POC_{aver}}\right)^2\right)}. \quad [5]$$

The coefficient of variance was calculated as a pooled sample:

$$cv_{r-O2:C} = \frac{\sigma_{r-O2:C}}{r_{-O2:C,aver}}. \quad [6]$$

Statistical linear models were fitted using one or two predictor variables (temperature [°C; T], nutricline depth [m; Z_{NO3} = 1 μM NO_3], phosphate [P], and N* [N* = [NO3] − 16*[P] + 2.9 mmol/m^3]). To evaluate assumptions of a normal-distributed respiration quotient, we also did a one-way multivariate analysis of variance (MANOVA) test. Here we evaluated the joint variance in POC and PCOD between the nine defined regions. We rejected the hypothesis that the data could be described in one dimension (i.e., a single mean $r_{-O2:C}$) and instead showed significant regional variability.

Our standard POM assay quantifies particles less than 30 μm to avoid the stochastic presence of rare large particles. However, large phytoplankton are an important contributor to POM in the Southern Ocean. To address any uncertainties with size selection, we also collected POM with no size fractionation between 54°S and 69°S (*SI Appendix*, Fig. S7*A*). We found that total [POC] or [PCOD] were only significantly different from the <30 μm fraction at a few stations. Furthermore, $r_{-O2:C}$ was not statistically different between the total and below <30 μm fractions. This suggested that capping the POM sample at a particle size of 30 μm did not affect the outcome of our analysis (*SI Appendix*, Fig. S7*C*).

Prognostic CESM Simulations. A modified version of CESM was used for our 300 y simulations, which included a prescribed $r_{-O2:C}$ranging between 0.7 and 1.3 across model experiments. Only a fixed $r_{-O2:C}$ value varied between these simulations. Climate forcings on the oceans followed a repeated cycling of the National Centers for Environmental Prediction–National Center for Atmospheric Research Reanalysis datasets for the years 1980 to 2009. Three hundred years is sufficient to spin up the upper ocean and thermocline depth nutrients and oxygen. Model output was averaged over the last 20 simulation years for analysis to remove short-term variability. The model includes three phytoplankton functional groups (small, large, and diazotrophic phytoplankton) and multiple potentially growth-limiting nutrients (N, P, Fe, and Si). The model has been used in CESM climate simulations (36, 37). The ecosystem–biogeochemistry model code is a preliminary version of the CESM V2.1 code set, run within the coarse-resolution CESM V1.2.2 ocean circulation model (19). Water column denitrification is initiated in the model when oxygen levels fall below 7 μM, with only denitrification and no oxic remineralization below 5 μM (36). Additional documentation and model source code for CESM2.0 are available online (www2.cesm.ucar.edu).

Analysis of CMIP5 Model Output. We obtained output from the Coupled Model Intercomparison Project Phase 5 (CMIP5) models from the Earth System Grid Federation (38). We calculated the changes in ocean oxygen content and rates of denitrification between the simulated 1990s and 2090s for available biogeochemical models following the historical and RCP8.5. This is the high-end, business as usual emissions scenario with strong global warming over the 21st century.

Inverse Hydrographic Model Analysis. See *SI Appendix* for a detailed description of the inverse model analysis.

Data Availability. The hydrography (39) and POM data (40) are freely available.

ACKNOWLEDGMENTS. We thank the captain and crew of the R/V *Ronald H. Brown*, the chief scientists B. Carter and R. Sonnerup, and the science party on board the P18 cruise. We also thank GO-SHIP coordinators Lynne Talley and Gregory Johnson for their support in participating in the US Global Ocean Carbon and Repeat Hydrography Program. This research was developed as part of A.R.M.'s dissertation "Biological Controls and Biogeochemical Outcomes of Marine Elemental Stoichiometry." Funding was provided by the NSF Graduate Research Fellowship Program and University of California,

Irvine Chancellor's Club Fellowship to A.R.M.; OCE-1848576 and OCE-1948842 to A.C.M. and F.W.P.; NASA Earth and Space Science Fellowship NESSF16R to C.A.G.; and US Department of Energy Office of Biological and Environmental Research awards DE-SC0016329, DE-SC0016539, and Reducing Uncertainties in Biogeochemical Interactions through Synthesis and Computation (RUBISCO) Scientific Focus Area to J.K.M.

1. S. Schmidtko, L. Stramma, M. Visbeck, Decline in global oceanic oxygen content during the past five decades. *Nature* **542**, 335–339 (2017).
2. R. J. Diaz, R. Rosenberg, Spreading dead zones and consequences for marine ecosystems. *Science* **321**, 926–929 (2008).
3. R. E. Keeling, A. Körtzinger, N. Gruber, Ocean deoxygenation in a warming world. *Annu. Rev. Mar. Sci.* **2**, 199–229 (2010).
4. L. Stramma, A. Oschlies, S. Schmidtko, Mismatch between observed and modeled trends in dissolved upper-ocean oxygen over the last 50 yr. *Biogeosciences* **9**, 4045–4059 (2012).
5. A. Oschlies, P. Brandt, L. Stramma, S. Schmidtko, Drivers and mechanisms of ocean deoxygenation. *Nat. Geosci.* **11**, 467–473 (2018).
6. A. Paulmier, I. Kriest, A. Oschlies, Stoichiometries of remineralisation and denitrification in global biogeochemical ocean models. *Biogeosciences* **6**, 923–935 (2009).
7. A. C. Redfield, B. H. Ketchum, F. A. Richards, "The influence of organisms on the composition of sea-water" in *The Sea*, M. N. Hill, Ed. (John Wiley, 1963), vol. 2, pp. 26–77.
8. L. A. Anderson, On the hydrogen and oxygen content of marine phytoplankton. *Deep Sea Res. Part I Oceanogr. Res. Pap.* **42**, 1675–1680 (1995).
9. E. A. Laws, P. G. Falkowski, W. O. Smith, H. Ducklow, J. J. McCarthy, Temperature effects on export production in the open ocean. *Global Biogeochem. Cycles* **14**, 1231–1246 (2000).
10. T. Tanioka, K. Matsumoto, Stability of marine organic matter respiration stoichiometry. *Geophys. Res. Lett.* **47**, e2019GL085564 (2020).
11. Z. V. Finkel *et al*., Phylogenetic diversity in the macromolecular composition of microalgae. *PLoS One* **11**, e0155977 (2016).
12. F. Fraga, A. F. Rios, F. F. Perez, F. G. Figueiras, Theoretical limits of oxygen:carbon and oxygen:nitrogen ratios during photosynthesis and the mineralization of the organic matter inthe sea. *Sci. Mar.* **62**, 161–168 (1998).
13. C. T. A. Chen, C. M. Lin, B. T. Huang, L. F. Chang, Stoichiometry of carbon, hydrogen, nitrogen, sulfur and oxygen in the particulate matter of the western North Pacific marginal seas. *Mar. Chem.* **54**, 179–190 (1996).
14. J. I. Hedges *et al*., The biochemical and elemental compositions of marine plankton: A NMR perspective. *Mar. Chem.* **78**, 47–63 (2002).
15. Y.-H. Li, T.-H. Peng, Latitudinal change of remineralization ratios in the oceans and its implication for nutrient cycles. *Global Biogeochem. Cycles* **16**, 77–1–77–16 (2002).
16. B. Schneider, J. Karstensen, A. Oschlies, R. Schlitzer, Model-based evaluation of methods to determine C:N and N:P regeneration ratios from dissolved nutrients. *Global Biogeochem. Cycles* **19**, 1–18 (2005).
17. T. DeVries, C. Deutsch, Large-scale variations in the stoichiometry of marine organic matter respiration. *Nat. Geosci.* **7**, 890–894 (2014).
18. Y.-C. Teng, F. W. Primeau, J. K. Moore, M. W. Lomas, A. C. Martiny, Global-scale variations of the ratios of carbon to phosphorus in exported marine organic matter. *Nat. Geosci.* **7**, 895–898 (2014).
19. W. L. Wang, J. K. Moore, A. C. Martiny, F. W. Primeau, Convergent estimates of marine nitrogen fixation. *Nature* **566**, 205–211 (2019).
20. I. Vyrides, D. C. Stuckey, A modified method for the determination of chemical oxygen demand (COD) for samples with high salinity and low organics. *Bioresour. Technol.* **100**, 979–982 (2009).
21. R. M. Key *et al*, Global Ocean Data Analysis Project (Version 2, GLODAPv2, 2015). https://www.glodap.info/. Accessed 14 December 2015.
22. A. Olsen *et al*., The Global Ocean Data Analysis Project version 2 (GLODAPv2)—An internally consistent data product for the world ocean. *Earth Syst. Sci. Data* **8**, 297–323 (2016).
23. F. W. Primeau, M. Holzer, T. DeVries, Southern Ocean nutrient trapping and the efficiency of the biological pump. *J. Geophys. Res.* **118**, 2547–2564 (2013).
24. D. M. Karl, E. Grabowski, The importance of H in particulate organic matter stoichiometry, export and energy flow. *Front. Microbiol.* **8**, 826 (2017).
25. T. Platt, B. Irwin, Caloric content of phytoplankton. *Limnol. Oceanogr.* **18**, 306–310 (1972).
26. J. I. Hedges *et al*., The molecularly-uncharacterized component of nonliving organic matter in natural environments. *Org. Geochem.* **31**, 945–958 (2000).
27. Z. V. Finkel, M. J. Follows, A. J. Irwin, Size-scaling of macromolecules and chemical energy content in the eukaryotic microalgae. *J. Plankton Res.* **38**, 1151–1162 (2016).
28. N. S. Shifrin, S. W. Chisholm, Phytoplankton lipids: Interspecific differences and effects of nitrate, silicate and light-dark cycles. *J. Phycol.* **17**, 374–384 (1981).
29. S. Roshan, T. DeVries, Efficient dissolved organic carbon production and export in the oligotrophic ocean. *Nat. Commun.* **8**, 2036 (2017).
30. J. B. Palter, M. S. Lozier, R. T. Barber, The effect of advection on the nutrient reservoir in the North Atlantic subtropical gyre. *Nature* **437**, 687–692 (2005).
31. W. A. Moore, R. C. Kroner, C. C. Ruchhoft, Dichromate reflux method for determination of oxygen consumed. *Anal. Chem.* **21**, 953–957 (1949).
32. F. J. Baumann, Dichromate reflux chemical oxygen demand. Proposed method for chloride correction in highly saline wastes. *Anal. Chem.* **46**, 1336–1338 (1974).
33. R. A. Dobbs, R. T. Williams, Elimination of chloride interference in the chemical oxygen demand test. *Anal. Chem.* **35**, 1064–1067 (1963).
34. J. R. Baker, M. W. Milke, J. R. Mihelcic, Relationship between chemical and theoretical oxygen demand for specific classes of organic chemicals. *Water Res.* **33**, 327–334 (1999).
35. Y.-C. Kim *et al*., Relationship between theoretical oxygen demand and photocatalytic chemical oxygen demand for specific classes of organic chemicals. *Analyst* **125**, 1915–1918 (2000).
36. J. K. Moore, K. Lindsay, S. C. Doney, M. C. Long, K. Misumi, Marine ecosystem dynamics and biogeochemical cycling in the Community Earth System Model [CESM1 (BGC)]: Comparison of the 1990s with the 2090s under the RCP4. 5 and RCP8. 5 scenarios. *J. Clim.* **26**, 9291–9312 (2013).
37. J. K. Moore *et al*., Sustained climate warming drives declining marine biological productivity. *Science* **359**, 1139–1143 (2018).
38. K. E. Taylor, R. J. Stouffer, G. A. Meehl, An overview of CMIP5 and the experiment design. *Bull. Am. Meteorol. Soc.* **93**, 485–498 (2012).
39. R. Sonnerup, B. Carter, S. Purkey, A. Bourbonnais, Data from "Hydrographic Cruise: 33RO20161119." CCHDO. Available at https://cchdo.ucsd.edu/cruise/33RO20161119. Accessed 12 August 2020.
40. A. C. Martiny, Line P18 POM concentrations. BCO-DMO. Available at https://www.bco-dmo.org/project/764270. Deposited 22 June 2020.